Published in final edited form as:

Nature. 2013 May 23; 497(7450): 521–524. doi:10.1038/nature12179.

Crystal structure of the integral membrane diacylglycerol kinase

Dianfan Li[1], **Joseph A. Lyons**[1], **Valerie E. Pye**[1,2], **Lutz Vogeley**[1], **David Aragão**[1,3], **Colin P. Kenyon**[4], **Syed T. A. Shah**[1], **Christine Doherty**[1,5], **Margaret Aherne**[1], and **Martin Caffrey**[1,*]

[1]School of Biochemistry and Immunology & School of Medicine, Trinity College Dublin, Dublin, Ireland [4]CSIR, Biosciences, Meiring-Naude Road, Pretoria, Gauteng, South Africa

Abstract

Diacylglycerol kinase (DgkA) catalyzes the ATP-dependent phosphorylation of diacylglycerol to phosphatidic acid for use in shuttling water-soluble components to membrane derived oligosaccharide and lipopolysaccharide in the cell envelope of Gram-negative bacteria[1]. For half a century, this 121-residue kinase has served as a paradigm for investigating membrane protein enzymology[1,3-7], folding[8,9], assembly[10-13], and stability[1,14]. Here, we present crystal structures for three functional forms of this unique and paradigmatic kinase, one of which is wild type (WT). These reveal a homo-trimeric enzyme with three transmembrane helices and an N-terminal amphiphilic helix per monomer. Bound lipid substrate and docked ATP identify the putative active site which is of the composite, shared site type. The crystal structures rationalize extensive biochemical and biophysical data on the enzyme. They are however at variance with a published solution NMR model[2] in that domain swapping, a key feature of the solution form, is not observed in the crystal structures.

DgkA is a unique enzyme, structurally and functionally. A solution NMR model of WT DgkA revealed a compact, domain-swapped trimer[2]. This, along with extensive biochemical and biophysical data, was used to rationalize its stability, folding, active site architecture, catalytic mechanism, and substrate selectivity. Because it was a backbone only model, with motional disorder over its first 25 residues, there was a need for a high resolution crystal structure. Traditional crystallization approaches had failed to produce quality crystals[15].

---

*Correspondence and requests for materials should be addressed to M.C. (martin.caffrey@tcd.ie).
[2]Present address: Clare Hall Laboratories, Cancer Research UK, Blanche Lane, South Mimms, Hertfordshire, EN6 3LD, UK.
[3]Present address: Australian Synchrotron, 800 Blackburn Road, Clayton, Victoria, VIC 3168, Australia.
[5]Present address: The Matrix Biology Group, Kennedy Institute of Rheumatology, University of Oxford, 65 Aspenlea Road, Hammersmith, London, W6 8LH, UK.

Author Information: Atomic coordinates and structure factors for WT, Δ4 and Δ7 DgkA are deposited in the Protein Data Bank (accession codes 3ZE4, 3ZE5, and 3ZE3, respectively).

Supplementary Information is linked to the online version of the paper at www.nature.com/nature.

Author Contributions D.L. produced, purified, crystallized and functionally characterized the protein and its variants, collected and processed diffraction data, refined and analysed the structures, and helped write the manuscript. J.A.L., D.A. and V.E.P. collected and processed data, solved, refined and analysed the structures, and helped write the manuscript. L.V. helped process data, solve and analyze structures and write the manuscript. M.A., C.D, and V.E.P. helped with protein and crystal production. C.K. performed docking. S.T.A.S provided 7.8 MAG for crystallization. M.C. was responsible for the overall project strategy and management and oversaw manuscript preparation.

Given the success of the lipidic cubic phase (*in meso*) method with similarly sized proteins[16], it was considered a worthwhile crystallization strategy.

Initial trials yielded minute crystals with monoolein (9.9 MAG) as host lipid at 20 °C. Rounds of optimization with shorter chain monoacylglycerols (MAGs) using rationally designed mutant forms of the kinase provided quality crystals at 4 °C. Molecular replacement (MR) with the published model[2] as template failed to provide a solution. To phase the X-ray data, seleno-methionine (Se-Met), as well as heavy atom pre-labelling, co-crystallization, and soaking, and engineered single-cysteine mutants for mercury labelling, were tested. Phases were obtained using Se-Met SAD from crystals of a stable active mutant, Δ7 (7 changes relative to WT, Supplementary Figs. 1, 2). Structures for the WT and a thermo-stabilized Δ4 (4 changes relative to WT)[14] form of DgkA were obtained by MR using the Δ7 structure (Online Methods). Here, we report on structures of the WT, Δ4 and Δ7 constructs obtained with 7.8 MAG. The highest resolution was for Δ7 DgkA at 2.05 Å (Supplementary Table 1).

The crystal structure of all three constructs reveals a trimer with layered packing (Fig. 1, Supplementary Fig. 3)[16]. Across constructs, subunits and folds are alike (Supplementary Figs. 4-6). This, coupled with the fact that the three constructs are active (Supplementary Fig. 2), indicates that all three are structurally and functionally similar. Δ4 provided the most complete model and is used for the structure description that follows.

Each subunit (identified A-C) within a trimer forms a bundle of 3 transmembrane helices, H1-3 (Fig. 1, Supplementary Fig. 7). When viewed from the cytosol, the centers of mass of the 3 helices within a subunit roughly describe an isosceles triangle (Fig. 1c). H1 is the shortest at 19 residues. It is preceded by an N-terminal amphiphilic surface helix (SH, Supplementary Fig. 6b) which is expected to reside on the cytosolic side of the membrane. H2 and H3 extend into the cell by about 10 residues and are connected by a ∼5-residue cytosolic loop (CL), likely to be quite mobile (Supplementary Fig. 5). On the other side of the membrane, H1 and H2 are connected by a 4 residue periplasmic loop (PL).

The three subunits are arranged around an approximate 3-fold symmetry axis that passes through the center of the trimer normal to the membrane plane (Fig. 1c). The core of the trimer is made up of H2 from each subunit forming a parallel 3-helix bundle. Extending away from the core, H1 and H3 from each subunit form the sides of an equilateral triangle that inscribes the trimer with H1 occupying apex positions. Viewed from the cytosol, the SH which is N-terminal to H1, angles away from the trimer core contacting H3 from an adjacent subunit. Together, the SH N-terminus of one subunit and H1-3 of an adjacent subunit create the putative active site (Fig. 1). Thus, for example, active site *AB* (as*AB*) is formed by SH_A, $H1_B$, $H2_B$ and $H3_B$, consistent with the composite, shared site model[5].

Separate studies have shown that the DgkA trimer has three active sites[5], with moderate heterollostery[1,4] (Supplementary Discussion). The enzyme has one amphiphilic substrate, DAG, and a water-soluble substrate, Mg^{2+}-ATP. Thus, DgkA catalyzes phosphoryl transfer expected to take place at a polar/apolar interface. Given that the reaction involves direct phosphorylation[4] via a pentavalent transition state, the two substrates must come into close

proximity with the γ-phosphate of ATP next to the primary hydroxyl of DAG. There is only one location (per active site) on the kinase where this can happen. That is in the pocket created by the SH of one subunit and the polar/apolar regions of H1-3 of an adjacent subunit (Fig. 1). This prediction matches well the active site residues mapped in previous studies[1,2] (Fig. 2).

DgkA is a promiscuous enzyme. It can work with different hydroxy lipids as substrates, including MAGs used to create the mesophase for crystallization[17-19]. One of the putative active sites in Δ7 includes density well described by MAG (Fig. 3, Supplementary Fig. 8). The lipid headgroup resides at the predicted membrane polar/apolar interface. Its acyl chain extends away from the interface into the hydrophobic membrane core next to H3. This tentatively identifies the lipid substrate half of a DgkA active site.

DgkA is a unique kinase with a distinctive active site. It has no recognizable nucleotide sequence or structural binding motifs[20,21]. With a view to identifying the ATP binding site, crystals of Δ7 DgkA were soaked with the ATP analog, adenylylmethylenediphosphate (Mg^{2+}-AMPPCP). This caused the crystals to 'dissolve' (Supplementary Fig. 9). Additional soaking with ATP, ADP, AMP, ATPγS, AMPPNP and dATP but not with GTP, CTP, UTP or TTP led to crystal dissolution (Supplementary Fig. 9). Thus, while a liganded structure did not materialize, the result is consistent with an adenine nucleotide-induced conformational and/or packing change in the crystalline kinase. These findings support the view that the kinase adopts a functional form in the crystal.

In the absence of a nucleotide-bound structure for DgkA, ATP has been docked into the Δ7 model with the adenyl moiety interacting with the CL (Fig. 3, Supplementary Discussion, Supplementary Fig. 10). The triphosphate extends in the direction of the lipid binding region of the putative active site, occupied by a lipid molecule. The observation of distinct binding sites, one (modelled) for ATP and one for the lipid substrate, is consistent with the finding that the mechanism of phosphoryl transfer is of the random-equilibrium type where the two substrates bind independently of one another[4,22].

For full activation, DgkA requires free divalent cation (magnesium, manganese, cadmium, zinc or cobalt)[23]. Here, zinc was found coordinated by the carboxyls of Glu 28 and Glu 76 (Supplementary Fig. 11) both vital to catalytic activity[2]. Superposing this onto the docked ATP-Δ7 DgkA structure positions the zinc 4.9 Å from the γ-phosphate (Fig. 3) where it may play a role in substrate placement for reaction.

The reaction product, phosphatidic acid, with its relatively bulky and charged phosphate, is expected to leave the active site for the surrounding membrane via the opening between the SH and H1 (Fig. 1). This may be facilitated electrostatically by Glu 69 and Glu 76 in H2 creating a push and by Arg 9 and Lys 12 in the SH creating a pull on the anionic product (Supplementary Fig. 12). All four residues are important for activity.

Lau *et al.*[5], using subunit mixing/complementarity experiments, provided evidence for shared sites in DgkA. Ala 14 and Glu 76 were identified as active site residues contributed from one subunit with Glu 69, Asn 72 and Lys 94 deriving from another.

The current structures show that the active sites are indeed composed of residues from two subunits consistent with the shared sites model (Fig. 1). For purposes of discussion, we focus on just one active site (as*BC*) (Supplementary Fig. 13). Highlighting the shared sites residues identified by Lau *et al.*[5], in this active site it is clear that Glu 69 and Asn 72 on $H2_C$ and Lys 94 on $H3_C$ are on one half-site while Ala 14 on SH_B is on the other. Glu 76 however is on H2. If it is to be on the same half-site as Ala 14 then it must be on $H2_B$ which is in as*AB*, not as*BC*. The current structure therefore is consistent with Ala 14 residing on one of the shared half-sites and Glu 69, Asn 72 and Lys 94 on the other. It is for these that maximum complementation was observed. For Glu 76, the experimental data were less convincing[5].

In the previous study[5] Asp 95 was shown to influence at least two active sites. For purposes of rationalizing this observation we focus on as*BC* and as*AB* (Supplementary Fig. 13). Asp 95 in $H3_C$ contacts SH_B which bridges two active sites. Its N-terminus contributes to as*BC* while its C-terminus, which extends into $H1_B$, contributes to as*AB*. Thus, modifying Asp 95 is likely to affect SH_B which, in turn, will influence both as*BC* and as*AB* consistent with the experimental observation[5].

The only other model for DgkA with which to compare our crystal structures was determined using solution NMR[2] and the two are different (Fig. 4). The biggest disparity relates to domain swapping which is present in the solution but not in the crystal structure. In the former, H3 from one subunit contacts H1 and H2 from an adjacent subunit in classic domain swapped fashion (Fig. 4a). The active site, in turn, is mapped to the space created by H1 and H3 from one subunit and H2 from another. As a result of these disparate quaternary structures, the architecture and chemistry of the active sites in the two models differ dramatically (Fig. 4; Supplementary Discussion). Interestingly, both are consistent with the shared sites model but for different reasons.

From the quality of the diffraction data and the corresponding refinement statistics (Supplementary Table 1) it is evident that the structures reported here faithfully represent what exists in the crystal. We must consider then if the crystal structure described is physiological because it is possible for crystal lattice restraints to impose unusual and perhaps even unnatural conformations. However, we report here two different crystal packing arrangements and the overall fold of the protein is the same in both. Further, we have obtained a crystal structure of the enzyme with lipid substrate binding sites occupied, modelled ATP into the binding site, found the enzyme is active under crystallization conditions and upon crystal dissolution (Supplementary Fig. 14), and have seen nucleotide and ATP analog soaking cause crystals to dissolve suggesting an adenine-specific, ligand-induced conformational change. All point to a protein with a functional form in the crystal. The solution structure, by contrast, is a low resolution, composite model that traces only the protein backbone. It was arrived at using connectivity and distance spectroscopic and cross-linking measurements, the tolerances of which can be considerable[2] (Supplementary Discussion, Supplementary Table 2, Supplementary Fig. 15). Presumably, long range distance restraints, as defined by residual dipolar couplings and paramagnetic resonance enhancements which have an inherent ambiguity, were used to assist in positioning swapped domains in the micellarized trimer. Because subunit and indeed atom ambiguity in

symmetric homo-oligomeric assemblies are complications inherent to structure determination by NMR[24,25], the possibility that the solution structure of DgkA is so affected cannot be ruled out.

DgkA is a unique kinase whose detailed catalytic mechanism has not been established. With the crystal structures reported here, a rational testing of hypotheses relating to mechanism can now be undertaken. DgkA is likely activated *in vivo* under hypo-osmotic conditions[4]. Activation contributes to enhanced production of the osmoregulant, membrane derived oligosaccharide. The physicochemical properties of membranes change in response to osmotic stress. We speculate that the SH connected to MH1 by a short hinge (Fig. 1) acts as a sensor of osmotic stress by responding to bilayer thickness and lateral pressure. Given that the SH is a part of the putative active site, adjustments in its conformation and position relative to H1 and to the rest of the trimer as the membrane responds to hypo-osmotic stress will alter active site architecture leading to enhanced kinase activity.

Methods

Protein

The *dgkA* wild-type gene and a *dgkA* mutant gene encoding for a thermostable quadruple mutant Δ4 DgkA (I53C, I70L, M96L, V107D)[14] were synthesized (Genescript) and cloned into pTrcHisB using *Nco*I and *Eco*RI restriction enzyme sites. A septuple variant, Δ7 DgkA (A41C, C46A, I53V, I70L, M96L, V107D, C113A) was generated using PCR-based site-directed mutagenesis and was verified by DNA sequencing.

DgkA native proteins were produced as described[19] with an additional size exclusion chromatography step. Se-Met labelling of Δ7 DgkA was performed following an established protocol using the methionine auxotroph B893(DE3) strain in M9 minimal media supplemented with Se-Met[29]. Selenium incorporation into DgkA proteins was verified by mass spectrometry.

Enzyme assays

For the stability assay of DgkA proteins, a coupled assay was used to monitor kinase activity. The consumption of ATP in the phosphorylation of monoolein was coupled through the sequential action of pyruvate kinase and lactate dehydrogenase to the oxidation of NADH monitored by a change in A_{340}, as described[4,19]. The assay mix contained 21 mM decylmaltoside, 7.2 mM monooolein (as substrate), 1.7 mM cardiolipin, 0.1 mM EGTA, 0.1 mM EDTA, 1 mM phosphenolpyruvate, 3 mM ATP, 15 mM magnesium acetate, 50 mM LiCl, 0.2 mM DTT, 0.3 mM NADH, 20 U/mL each of pyruvate kinase and lactate dehydrogenase, 75 mM PIPES pH 6.9. The assays were run at 0.25 μg DgkA protein/mL in 384-well plates.

To assay Δ7 DgkA activity under crystallization conditions, 20 μL mesophase, formed by mixing 10 μL DgkA solution (12 mg/mL) and 10 mg 7.8 MAG, was bathed in 1 mL crystallization precipitant (4.5 %(v/v) MPD, 0.1 M sodium chloride, 60 mM magnesium acetate, 50 mM sodium citrate pH 5.6) supplemented with 10 mM ATP. After incubating at 4 °C for 0, 0.5, 1, 2, 3, 5 and 10 h, 3 μL of the bathing solution was removed and transferred

to 60 μL ADP assay mix (0.2 mM NADH, 1 mM phosphenolpyruvate, 15 mM magnesium chloride, 20 U/mL each of pyruvate kinase and lactate dehydrogenase, 75 mM PIPES pH 6.9) in a 384-well plate. After incubation for 10 min at 30 °C, the drop in A_{340} of the well contents was used to calculate activity. Control measurements were made using protein-free buffer. Assays were run in triplicate.

Crystallization

In meso crystallization trials began with the reconstitution of the protein into the bilayer of the lipidic cubic mesophase. This was done following a standard protocol[30]. The protein solution at 12 mg/mL was homogenized with 7.8 MAG in equal parts by volume using a coupled syringe device at room temperature (RT, 20 - 22 °C). Crystallization trials were set up by transferring 50 nL of the protein/lipid cubic mesophase onto a silanized 96-well glass crystallization plate which was subsequently covered with 800 nL precipitant solution using *in meso* robots[31]. Wells were sealed with a glass coverslide. The glass sandwich plates were stored in a walk-in refrigerator at 4-6 °C for crystal growth. Crystallization progress was monitored using normal and cross-polarized light microscopy (Eclipse E 400 Pol, Nikon, Melville, NY) at 4-6 °C. Precipitant solutions consisted of 4-6 %(v/v) MPD, 0.1 M sodium chloride, 0.1 M lithium nitrate, 60 mM magnesium acetate, and 50 mM sodium citrate pH 5.6 for WT and Δ4 DgkA. Lithium nitrate was not used for Δ7 DgkA crystallization. Bipyramid shaped crystals grew to a maximum size of 50 × 50 × 50 μm^3 and 50 × 75 ×100 μm^3 in 45-60 d for WT and Δ4 DgkA, respectively. For Δ7 DgkA, rectangular crystals grew to a maximum size of 10 × 50 × 150 μm^3 in 45-60 days (Supplementary Fig. 9). Wells were opened with a tungsten-carbide glass cutter (Silverline) and the crystals were harvested using 30 - 100 μm micromounts (MiTeGen) at 4-6 °C. Crystals were snap-cooled directly in liquid nitrogen[32].

Crystal soaking *in situ* was carried out by cutting a window in the coverglass of the *in meso* crystallisation sandwich plate and injecting through it a solution containing nucleotide, nucleotide analogue or glutaraldehyde into the precipitant solution bathing the mesophase. When a second soaking was required excess bathing solution was wicked away with tissue paper[32], fresh solution with or without additive was added through the window, and the well was sealed with ClearSeal film (Hampton). Crystals were harvested as described above.

Data collection and processing

X-ray diffraction data were collected on the 23-ID-B beamline of the General Medicine and Cancer Institutes Collaborative Access Team (GM/CA-CAT) at the Advanced Photon Source (APS), Argonne, Illinois, USA, and the I24 beamline at the Diamond Light Source (DLS), Didcot, Oxford. Data were collected using a 10 μm collimated minibeam at GM/CA-CAT[33], while a 10 μm microfocus beam was used at DLS[34]. Diffraction images taken with a 10-fold attenuated beam were used to locate and centre on highly ordered regions of the crystal[35]. For the high resolution data set collected on crystals of Δ7 DgkA, the data reduction strategy involved combining a complete low resolution (3.0 Å) data set recorded from a single crystal with eighteen high resolution 10° wedges of data collected from multiple crystals.

Data were reduced with xia2[36] using XDS[37], XSCALE and SCALA[38]. Optimum data wedges were identified by data quality and isomorphic unit cell parameters. These data were rescaled in XSCALE and merged in SCALA (Supplementary Table 1). Similarly, a 200-fold redundant anomalous Se-Met data set to 3.0 Å resolution was obtained by merging 19 data sets. Complete datasets for Δ4 DgkA and WT were obtained from single crystals which were reduced with xia2 as outlined above.

Structure solution and refinement

Molecular replacement (MR) with the published NMR model[2] as template failed to provide a solution. Wide-search MR[39]against every known protein fold, and BALBES[40], also failed to provide a solution. The structure of Δ7 DgkA was determined by SAD phasing using the anomalous contributions of the Se-Met derivative[41]. Seventeen potential selenium sites were identified and refined with SHELX CDE[42] yielding a pseudo-free correlation coefficient of 65 %. Phases were extended to the native 2.05 Å data set using Phenix[43]. The initial model was built with Phenix Autobuild and yielded an initial model of 440 residues that gave an R_{free} of 0.35. It was evident that the asymmetric unit contained two trimers of DgkA. The final structure was attained by iterative model building in Coot[44] and refinement with Phenix.refine[43]. Optimal weights between X-ray target and stereochemistry were assigned automatically in Phenix.refine. Density modification and solvent flattening were recalculated on a regular basis until the maps showed minimal improvements. Se-Met phases were included throughout the majority of the refinement but then were excluded for the final rounds of refinement due to marginal anisotropy between the Se-Met and native data. Non-crystallographic symmetry (NCS) restraints were not used as the polypeptide chains varied to a reasonable extent within the asymmetric unit. TLS groups were used in the latter stages of refinement, two groups per chain, as identified using the TLSMD server[45].

Initial phases for Δ4 DgkA were obtained by molecular replacement as performed by the program Phaser[46] using the more complete trimer of the Δ7 DgkA model (Chains A-C). In subsequent cycles of iterative model building and refinement the programs Coot and O[47] were used for model building while the programs Buster[48] and Phenix were used for refinement in the initial and later stages, respectively. Refinement in Buster was performed with automatic NCS determination, while NCS was not used for refinement in Phenix. Four TLS groups per chain were generated using the TLSMD web server and used by both refinement programs.

Initial phases for WT DgkA were obtained as above for Δ4 DgkA using the Δ4 DgkA model. The program Coot was employed for model building while the program Phenix was used for refinement. NCS was used throughout the refinement. TLS groups (9 for Chain A, 4 for Chain B and 2 for Chain A) were generated using Phenix and were used throughout the refinement.

Lipid, crystallisation reagents, and unassigned density

Electron density for a total of 13 lipid molecules (both enantiomers of 7.8 1-MAG) were identified in a composite omit 2Fo-Fc map of Δ7 DgkA. Acetate and citrate molecules were

similarly identified and modelled in the electron density map. Tentatively modelled lipid and solvent molecules were removed if no clear hydrogen bonding was present and/or the model was not justified by the electron density.

Zinc

The location of a single metal ion in the asymmetric unit was determined in a Fo-Fc map of Δ7 DgkA. The ion identity was confirmed by X-ray fluorescence spectroscopy of crystals and an anomalous difference map generated from X-ray diffraction data collected at the zinc edge (9.6767 keV, Supplementary Table 1, Supplementary Fig. 11).

Water

In the Δ7 DgkA model, water molecules were assigned based on sigma-A weighted 2Fo-Fc electron density maps contoured at 1σ using standard geometrical and chemical restraints, for a total of 188 water molecules per asymmetric unit.

Electrostatics

The electrostatic surface potentials for DgkA were calculated using the Advanced Poisson-Boltzmann Solver (APBS) plugin, as implemented in PyMol, using default parameters[49].

Docking

ATP is ∼20 Å long, equalling the distance between CL and the primary hydroxyl of the putative lipid substrate in Δ7 DgkA. ATP with varying α/β/γ-phosphate protonation was docked into energy minimized Δ7 DgkA (Lys 12 unprotonated, Mg^{2+} coordinated to Asn 72 and Glu 76) using LibDock[50]. Poses with the highest LibDock scores were energy minimized to zero energy over 2,000 steps using the Smart minimizer with a Generalized Born with Molecular Volume implicit solvent model (Discovery Studio 3.5, Accelrys, CA, USA). The optimum pose was selected based on coordination with CL, lipid substrate, Mg^{2+}, and putative active site residues, Lys 12 and Lys 94.

Protein figures were generated and rendered in PyMOL.

Supplementary Material

Refer to Web version on PubMed Central for supplementary material.

Acknowledgments

We acknowledge support from Science Foundation Ireland Grants 07/IN.1/B1836 and 12/IA/1255, and the National Institutes of Health Grants GM75915, P50GM073210, U54GM094599, and FP7 COST CM0902. We thank C. R. Sanders for providing *E. coli* strain WH1061. The assistance and support of beamline scientists at the Advanced Photon Source (23-ID) and Diamond Light Source (I24) are gratefully acknowledged. We thank R. Sanishvili for assistance with zinc analysis, C. Boland and J. Tan for help with diffraction data collection, and A. Coughlan for help with lipid synthesis.

References

1. Van Horn WD, Sanders CR. Prokaryotic diacylglycerol kinase and undecaprenol kinase. Annu Rev Biophys. 2012; 41:81–101. [PubMed: 22224599]

2. Van Horn WD, et al. Solution nuclear magnetic resonance structure of membrane-integral diacylglycerol kinase. Science. 2009; 324:1726–1729. [PubMed: 19556511]
3. Schneider EG, Kennedy EP. Phosphorylation of ceramide by diglyceride kinase preparations from *Escherichia coli*. J Biol Chem. 1973; 248:3739–3741. [PubMed: 4573983]
4. Badola P, Sanders CR. Escherichia coli diacylglycerol kinase is an evolutionarily optimized membrane enzyme and catalyzes direct phosphoryl transfer. J Biol Chem. 1997; 272:24176–24182. [PubMed: 9305868]
5. Lau FW, Chen X, Bowie JU. Active sites of diacylglycerol kinase from *Escherichia coli* are shared between subunits. Biochemistry. 1999; 38:5521–5527. [PubMed: 10220339]
6. Pilot JD, East JM, Lee AG. Effects of bilayer thickness on the activity of diacylglycerol kinase of *Escherichia coli*. Biochemistry. 2001; 40:8188–8195. [PubMed: 11444964]
7. Lahiri S, Brehs M, Olschewski D, Becker CF. Total chemical synthesis of an integral membrane enzyme: diacylglycerol kinase from *Escherichia coli*. Angew Chem Int Ed Engl. 2011; 50:3988–3992. [PubMed: 21433227]
8. Sanders CR, et al. *Escherichia coli* diacylglycerol kinase is an alpha-helical polytopic membrane protein and can spontaneously insert into preformed lipid vesicles. Biochemistry. 1996; 35:8610–8618. [PubMed: 8679623]
9. Gorzelle BM, et al. Reconstitutive refolding of diacylglycerol kinase, an integral membrane protein. Biochemistry. 1999; 38:16373–16382. [PubMed: 10587463]
10. Vinogradova O, Badola P, Czerski L, Sonnichsen FD, Sanders CR. *Escherichia coli* diacylglycerol kinase: a case study in the application of solution NMR methods to an integral membrane protein. Biophys J. 1997; 72:2688–2701. [PubMed: 9168044]
11. Nagy JK, Lau FW, Bowie JU, Sanders CR. Mapping the oligomeric interface of diacylglycerol kinase by engineered thiol cross-linking: homologous sites in the transmembrane domain. Biochemistry. 2000; 39:4154–4164. [PubMed: 10747807]
12. Wen J, Chen X, Bowie JU. Exploring the allowed sequence space of a membrane protein. Nat Struct Biol. 1996; 3:141–148. [PubMed: 8564540]
13. Smith RL, O'Toole JF, Maguire ME, Sanders CR. Membrane topology of *Escherichia coli* diacylglycerol kinase. J Bacteriol. 1994; 176:5459–5465. [PubMed: 8071224]
14. Zhou Y, Bowie JU. Building a thermostable membrane protein. J Biol Chem. 2000; 275:6975–6979. [PubMed: 10702260]
15. Lorch M, et al. How to prepare membrane proteins for solid-state NMR: A case study on the alpha-helical integral membrane protein diacylglycerol kinase from E. coli. Chembiochem. 2005; 6:1693–1700. [PubMed: 16138309]
16. Caffrey M, Li D, Dukkipati A. Membrane protein structure determination using crystallography and lipidic mesophases: recent advances and successes. Biochemistry. 2012; 51:6266–6288. [PubMed: 22783824]
17. Walsh JP, Fahrner L, Bell RM. sn-1,2-diacylglycerol kinase of *Escherichia coli*. Diacylglycerol analogues define specificity and mechanism. J Biol Chem. 1990; 265:4374–4381. [PubMed: 2155227]
18. Bohnenberger E, Sandermann H Jr. Lipid dependence of diacylglycerol kinase from *Escherichia coli*. Eur J Biochem. 1983; 132:645–650. [PubMed: 6303781]
19. Li D, Caffrey M. Lipid cubic phase as a membrane mimetic for integral membrane protein enzymes. Proc Natl Acad Sci U S A. 2011; 108:8639–8644. [PubMed: 21555546]
20. Matte, A.; Delbaere, LTJ. ATP-binding Motifs. eLS John Wiley & Sons, Ltd; 2001.
21. Krissinel E. On the relationship between sequence and structure similarities in proteomics. Bioinformatics. 2007; 23:717–723. [PubMed: 17242029]
22. Ullrich SJ, Hellmich UA, Ullrich S, Glaubitz C. Interfacial enzyme kinetics of a membrane bound kinase analyzed by real-time MAS-NMR. Nat Chem Biol. 2011; 7:263–270. [PubMed: 21423170]
23. Walsh JP, Bell RM. sn-1,2-Diacylglycerol kinase of *Escherichia coli*. Mixed micellar analysis of the phospholipid cofactor requirement and divalent cation dependence. J Biol Chem. 1986; 261:6239–6247. [PubMed: 3009449]

24. Martin JW, Yan AK, Bailey-Kellogg C, Zhou P, Donald BR. A geometric arrangement algorithm for structure determination of symmetric protein homo-oligomers from NOEs and RDCs. J Comput Biol. 2011; 18:1507–1523. [PubMed: 22035328]
25. Martin JW, Yan AK, Bailey-Kellogg C, Zhou P, Donald BR. A graphical method for analyzing distance restraints using residual dipolar couplings for structure determination of symmetric protein homo-oligomers. Protein Sci. 2011; 20:970–985. [PubMed: 21413097]
26. Caffrey, M.; Lyons, J.; Smyth, T.; Hart, DJ. Monoacylglycerols: The workhorse lipids for crystallizing membrane proteins in mesophases. In: DeLucas, L., editor. Current Topics in Membranes. Vol. 63. Academic Press; 2009. p. 83-108.Ch. 4
27. Coleman BE, et al. Modular Approach to the Synthesis of Unsaturated 1-Monoacyl Glycerols. Synlett. 2004; 20041339:1342.
28. Lomize MA, Pogozheva ID, Joo H, Mosberg HI, Lomize AL. OPM database and PPM web server: resources for positioning of proteins in membranes. Nucleic Acids Res. 2012; 40:370–376.
29. Doublie S. Production of selenomethionyl proteins in prokaryotic and eukaryotic expression systems. Methods Mol Biol. 2007; 363:91–108. [PubMed: 17272838]
30. Caffrey M, Porter C. Crystallizing Membrane Proteins for Structure Determination using Lipidic Mesophases. J Vis Exp. 2010; 45:e1712.
31. Li D, Boland C, Walsh K, Caffrey M. Use of a robot for high-throughput crystallization of membrane proteins in lipidic mesophases. J Vis Exp. 2012; 67:e4000. [PubMed: 22971907]
32. Li D, Boland C, Aragao D, Walsh K, Caffrey M. Harvesting and cryo-cooling crystals of membrane proteins grown in lipidic mesophases for structure determination by macromolecular crystallography. J Vis Exp. 2012; 67:e4001. [PubMed: 22971942]
33. Fischetti RF, et al. Mini-beam collimator enables microcrystallography experiments on standard beamlines. J Synchrotron Radiat. 2009; 16:217–225. [PubMed: 19240333]
34. Evans G, Axford D, Owen RL. The design of macromolecular crystallography diffraction experiments. Acta Crystallogr D. 2011; 67:261–270. [PubMed: 21460444]
35. Cherezov V, et al. Rastering strategy for screening and centring of microcrystal samples of human membrane proteins with a sub-10 microm size X-ray synchrotron beam. J R Soc Interface. 2009; 6(5):S587–597. [PubMed: 19535414]
36. Winter G. xia2: an expert system for macromolecular crystallography data reduction. J Appl Cryst. 2010; 43:186–190.
37. Kabsch W. XDS. Acta Crystallogr D. 2010; 66:125–132. [PubMed: 20124692]
38. Evans P. Scaling and assessment of data quality. Acta Crystallogr D. 2006; 62:72–82. [PubMed: 16369096]
39. Stokes-Rees I, Sliz P. Protein structure determination by exhaustive search of Protein Data Bank derived databases. Proc Natl Acad Sci U S A. 2010
40. Long F, Vagin AA, Young P, Murshudov GN. BALBES: a molecular-replacement pipeline. Acta Crystallogr D. 2008; 64:125–132. [PubMed: 18094476]
41. Hendrickson WA, Horton JR, LeMaster DM. Selenomethionyl proteins produced for analysis by multiwavelength anomalous diffraction (MAD): a vehicle for direct determination of three-dimensional structure. EMBO J. 1990; 9:1665–1672. [PubMed: 2184035]
42. Sheldrick GM. Experimental phasing with SHELXC/D/E: combining chain tracing with density modification. Acta Crystallogr D. 2010; 66:479–485. [PubMed: 20383001]
43. Adams PD, et al. PHENIX: a comprehensive Python-based system for macromolecular structure solution. Acta Crystallogr D. 2010; 66:213–221. [PubMed: 20124702]
44. Emsley P, Lohkamp B, Scott WG, Cowtan K. Features and development of Coot. Acta Crystallogr D. 2010; 66:486–501. [PubMed: 20383002]
45. Painter J, Merritt EA. TLSMD web server for the generation of multi-group TLS models. J Appl Crystallogr. 2006; 39:109–111.
46. McCoy AJ, et al. Phaser crystallographic software. J Appl Crystallogr. 2007; 40:658–674. [PubMed: 19461840]

47. Jones TA, Zou JY, Cowan SW, Kjeldgaard M. Improved methods for building protein models in electron density maps and the location of errors in these models. Acta Crystallogr A. 1991; 47:110–119. [PubMed: 2025413]

48. Blanc E, et al. Refinement of severely incomplete structures with maximum likelihood in BUSTER-TNT. Acta Crystallogr D. 2004; 60:2210–2221. [PubMed: 15572774]

49. Baker NA, Sept D, Joseph S, Holst MJ, McCammon JA. Electrostatics of nanosystems: application to microtubules and the ribosome. Proc Natl Acad Sci U S A. 2001; 98:10037–10041. [PubMed: 11517324]

50. Diller DJ, Merz KM Jr. High throughput docking for library design and library prioritization. Proteins. 2001; 43:113–124. [PubMed: 11276081]

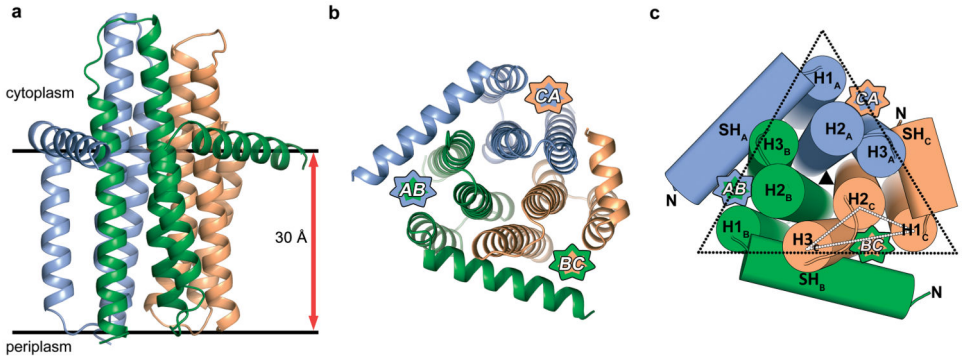

Figure 1. Crystal structure of Δ4 DgkA

a, Structure (ribbon model) viewed from the membrane plane. Individual subunits are coloured blue, green and orange. Membrane boundaries are based on hydrophobic thickness calculations from the PPM server[28]. **b**. As in **a**, viewed from the cytoplasm. Putative active sites are designated based on the identities of the subunits (A, B, C) contributing to each site and demarked with a seven pointed star. **c**. As in **b** with helices shown as cylinders and the structure notation introduced. The solid black triangle marks the axis of an approximate three-fold symmetry. Dotted triangles define the transmembrane helical core of the trimer (black) and the arrangement of transmembrane helices (H1-H3) in individual subunits (white). The N-terminus (N) in the model of each subunit is identified. It leads directly into an amphiphilic surface helix (SH) whose length varies between subunits.

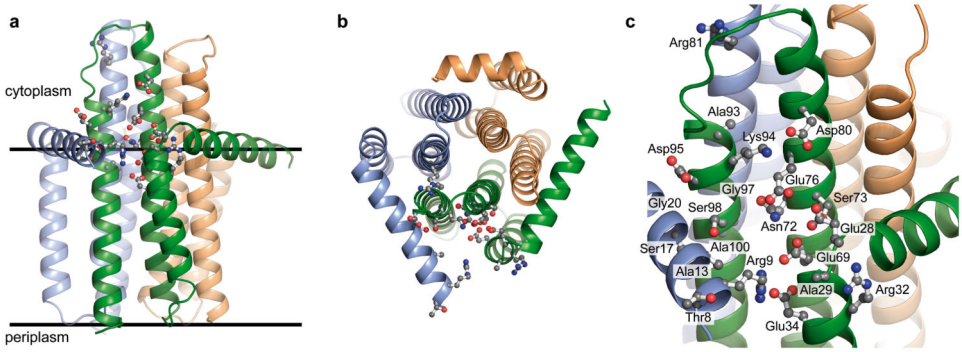

Figure 2. Rationalizing functional biochemistry with the crystal structure of DgkA

Residues in DgkA where mutations to cysteine reduce kinase activity to 7 % or less that of wild type activity[2] are mapped onto the crystal structure of Δ4 DgkA. **a**, View in the membrane plane. The protein (ribbon model) is displayed with chains A, B and C colored blue, green and orange, respectively. Residues are shown in ball and stick and color coded according to atom type (nitrogen, blue; oxygen, red; carbon, grey). **b**, View from the cytoplasm. **c**, An expanded view of the putative active site (as*AB*) of the enzyme, where residues critical to kinase activity[2] are clustered.

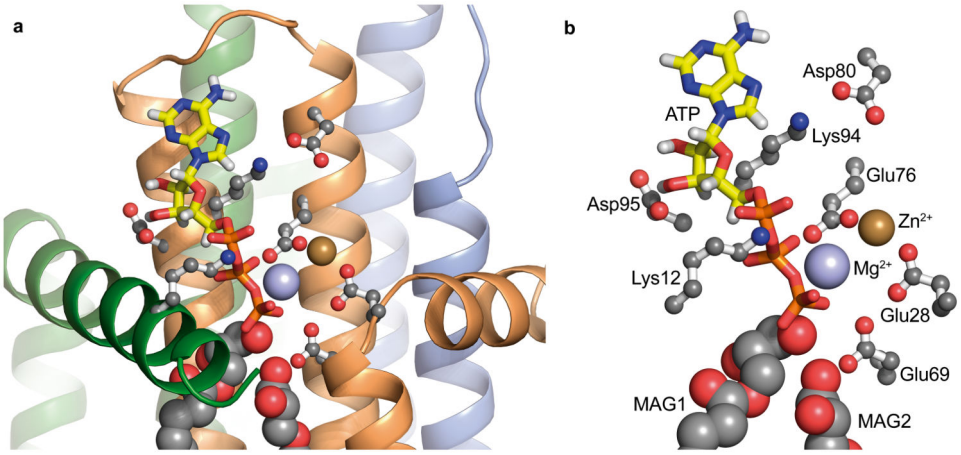

Figure 3. Putative active site of DgkA complete with lipid and Mg^{2+}-ATP substrates and activating zinc

a, A putative active site of Δ4 DgkA is shown superposed with 7.8 MAG lipid substrate, the zinc ion from Δ7 DgkA, and Mg^{2+}-ATP from the docking calculation. The ATP (thick sticks, atoms colored by type) extends ∼20 Å from the cytoplasmic loop between H2 and H3 to the polar headgroup of the lipid substrate (large spheres, atoms colored by type) at the polar/apolar interface of the membrane. Residues in the vicinity of the substrates that are known to be critical for kinase activity[2] are shown in ball and stick, as in Fig. 2. Zinc and magnesium are shown as brown and blue spheres, respectively. **b**, Expanded view of **a** with the ribbon model removed for clarity.

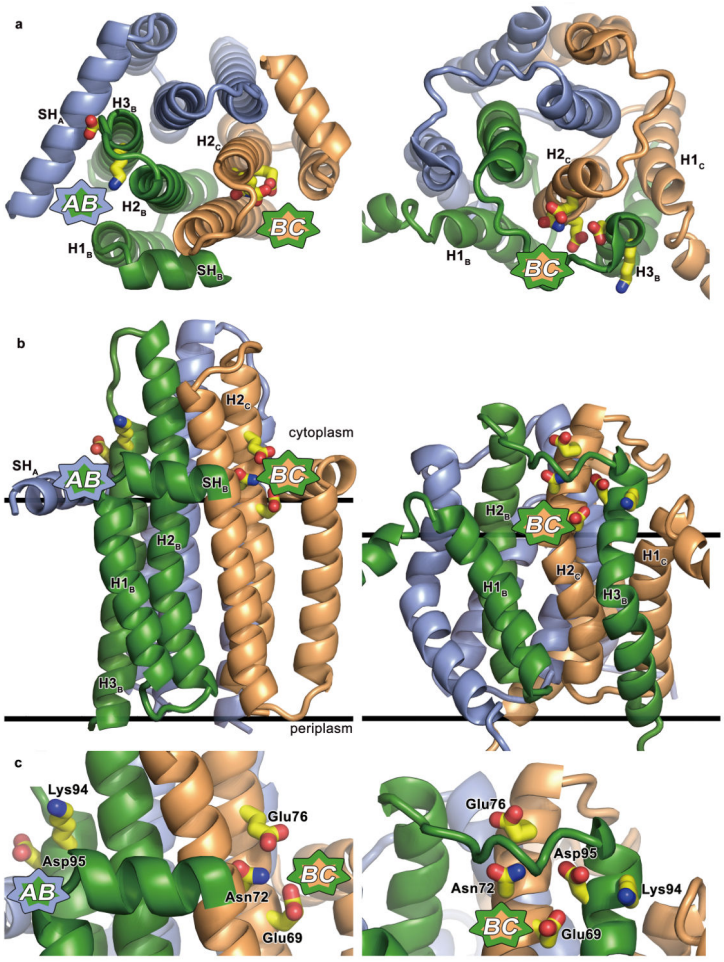

Figure 4. Comparison of the crystal and solution NMR structures of DgkA

A view of the crystal (left) and solution structures (right) from **a**, the cytoplasm, and **b**, the membrane plane. **c**, An expanded view of the putative active site region. The five most highly conserved residues and how they contribute to a single active site (as*BC*) in the solution structure are shown (right panels), as described by Van Horn *et al*.[2]. In the crystal structure, three of these five residues (Glu 69, Asn 72, Glu 76) contribute to one active site, as*BC*; two (Lys 94, Asp 95) are in as*AB*. The SH of the solution model, which is ill-defined, has been truncated for reasons of space. SH_B of the crystal structure has been trimmed at residue 18 to reveal the active site (as*BC*). Membrane boundaries are based on hydrophobic thickness calculations from the PPM server[28].